https://doi.org/10.2352/ISSN.2169-4451.2019.35.162

Advances in the Decoding of Data-Bearing Halftone Images*

Ziyi Zhao, Purdue University, West Lafayette, IN, USA
Robert Ulichney, Hewlett-Packard Co., Stow, MA, USA
Matthew Gaubatz, Hewlett-Packard Co., Seattle, WA, USA
Stephen Pollard, Hewlett-Packard Co., Bristol, UK
Jan P. Allebach, Purdue University, West Lafayette, IN, USA

Abstract

Data-bearing halftone images are an aesthetically pleasing alternative to barcodes. A frequency-based method has been proposed to determine the scale, orientation and the location of such images [1]. However, we find that the introduction of periodic shifting of halftone dots complicates the detection of fundamental peaks in the frequency domain. In order to analyze and solve the problem, we develop solutions based on mathematical analysis and simulation. We also perform experiments to detect the peaks in the frequency domain using camera-captured halftone images. Based on this work, a potential optimal design for data-bearing halftone images will be proposed enabling the fundamental peaks to be detected more accurately. We also provide a theoretical proof that this design is optimal.

Introduction

Data bearing halftone images [2] [3] [4] [5] are visually pleasant, and represent a high data density alternative to barcodes. In prior work [6], the alignment and recovery method for data bearing halftone designs has been introduced. Design parameters of a data-bearing halftone image, such as scale, orientation, and location, can be recovered using a frequency domain-based algorithm [1]. In the frequency domain, accurate detection of fundamental peaks is crucial for the subsequent algorithm to calculate the relevant parameters. In some experiments, we have observed false detection of the fundamental peaks. This observation has motivated us to theoretically explore the frequency-domain peak distribution.

Problem

Embedding machine-readable data in print has many uses, including authentication, labeling, and tracking. As an aesthetically pleasing alternative to barcodes, we use classical clustered-dot halftones with a periodic threshold array and embed data by shifting the centers of the dot clusters [2]. As part of the detection, we determine the scale and orientation of the halftone by finding the highest amplitude peak in the frequency domain, due to the strong periodic nature of this kind of halftone [1][7]. We recently determined that data payloads with long runs of similar shifts (i.e., long runs of ones or zeros) can make alignment difficult in data recovery, as the average centers of the clusters would have a bias. To remedy this issue, we introduce balanced shifting where the shift position for a cluster corresponding to a given bit will use a mix of shifts in opposite directions with equal distance from the center position. For example, a one bit would shift up or down, and a zero bit would shift left or right. This regular variation in shifting creates spectral energy that constructively interferes with higher harmonics of the fundamental. In the frequency domain, this modification can result in the highest peak not representing the fundamental frequency. In this paper, we analyze this problem and present a solution. The following notation is used to describe the problem and approach. The units for N, M, L, S, and T are printer-addressable pixels.

- g Halftone image in spatial domain
- G Halftone image in frequency domain
- N Halftone image width
- M Halftone cell width
- P $P = N/M$ Number of halftone cells across the width of the image
- L Clustered dots shift distance
- $S \times T$ Dot cluster size

In order to clearly illustrate the problem, we set image height equal to image width and (halftone) cell height equal to cell width. Inspired by Ulichney's analysis of blue noise using the radially averaged power spectrum (RAPS) [8], we adopt the radial maximum power spectrum (RMPS) to radially detect the peak magnitude distribution in the frequency domain. Figure 1 illustrates the RMPS for a particular choice parameter values and a particular payload. In this example, $N = 480$, $S = 2$, $T = 2$, $M = 24$, $L = 9$. We adopt balanced shifting rule using a random payload (a random binary sequence). We apply the DFT, and find the maximum peak at every radius in the frequency domain.

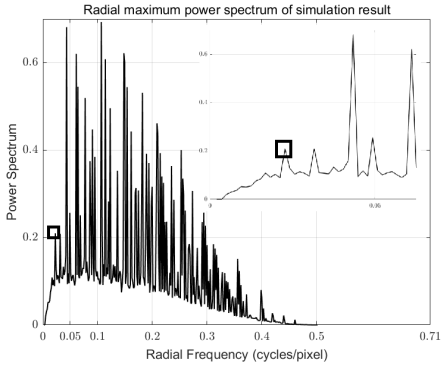

Figure 1. *Radial maximum power spectrum (RMPS) for an example halftone pattern with a random payload. The small box at the left identifies the peak corresponding to the fundamental frequency. Note that it is not the maximum peak in the RMPS. Note that the units are cycles/pixel in the digital halftone image*

*Research supported by HP Labs, Palo Alto, CA 94304.

This example shows that it is very hard for us to set a threshold to find the fundamental peaks directly because the magnitude of the fundamental peaks is quite small compared to other peaks. This has motivated us to explore the relationship between the peak distribution and the encoded image parameters

Theoretical Analysis

The data bearing halftone image consists of carrier halftone cells and abstention halftone cells [2][9]. In each carrier cell, the cluster shifts in a specific direction to encode a bit value (0 or 1) in the payload. In one example, a bit with value 1 would shift up or down, and a bit with value 0 would shift left or right. In each abstention halftone cell, there is no cluster. Figure 2 shows an example of a data-bearing halftone text document image. To decode the payload, use the region in halftone image shown in the black box in Figure 2 for analysis due to its reliability and reduced degree of noise due to non-constant content. The black box region corresponds to a fixed gray level background. Figure 3 is a close-up view of the black box region in Figure 2. For the purpose of analysis, we make the assumption that the payload is a random sequence consisting of 0s and 1s. For simulation, we generate a digital data-bearing halftone image using a random payload. Then the DFT is performed on the analysis region of the generated digital data-bearing halftone image.

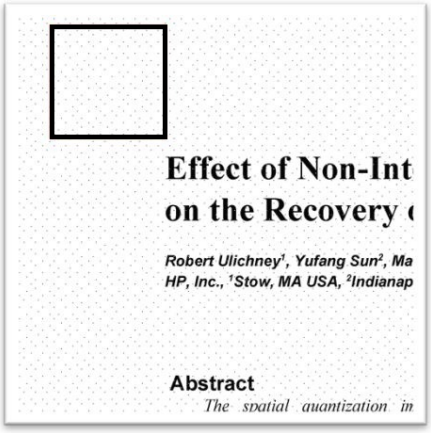

Figure 2. *Data-bearing halftone of a text document image.*

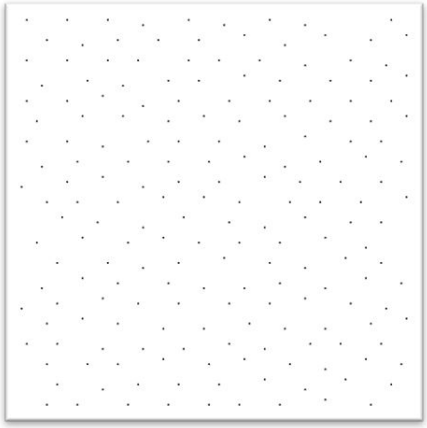

Figure 3. *Zoom-in of black box region from Figure 2.*

For the odd rows of halftone cells, the following notation is used to describe the balanced shifting rule proposed above:

X: Random variable describing the shifting direction of the dot cluster when encoding bit is 0 (X = 1: shift right, X = 0: no shift, X = -1: shift left)

Y: Random variable describing the shifting direction of the dot cluster when encoding bit is 1 (Y = 1: shift up, Y = 0: no shift, Y = -1: shift down)

Based on these assumptions, we establish a probability model for the balanced shifting rule.

$$\begin{aligned} P\left(X_{i,j}=1 \cup Y_{i,j}=0\right) &= \frac{1}{4} \\ P\left(X_{i,j}=-1 \cup Y_{i,j}=0\right) &= \frac{1}{4} \\ P\left(X_{i,j}=0 \cup Y_{i,j}=1\right) &= \frac{1}{4} \\ P\left(X_{i,j}=0 \cup Y_{i,j}=-1\right) &= \frac{1}{4} \end{aligned} \tag{1}$$

The probability distribution for an even row of halftone cells is the same as that for an odd row of halftone cells except that we denote the two random variables by U and V.

The data bearing halftone image in Figure 2 can be expressed in the following equation.

First, we define dot cluster function.

$$r[m,n] = \sum_{s=0}^{S-1}\sum_{t=0}^{T-1}\delta[m-s,n-t] \tag{2}$$

The spatial domain expression for the halftone image can then written as:

$$\begin{aligned} g[m,n] = &\sum_{i=0}^{\frac{P}{2}-1}\sum_{j=0}^{\frac{P}{2}-1} r[m-2i\cdot M-U_{i,j}L, n-2j\cdot M-V_{i,j}L] \\ &+ \sum_{i=0}^{\frac{P}{2}-1}\sum_{j=0}^{\frac{P}{2}-1} r[m-M-2i\cdot M-X_{i,j}L, n-M-2j\cdot M-Y_{i,j}L] \end{aligned} \tag{3}$$

Theoretically, we perform the Discrete Fourier Transform of the image in the spatial domain. Then, combined with the probabilistic model, we are able to determine the predicted peak distributions in the frequency domain. The expectation of the magnitude of $G[k,l]$ is as follows.

$$\mathscr{E}(|G(k,l)|) = \begin{cases} \frac{1}{2}P^2\cdot f_1(k,l)\cdot f_2(k,l)\cdot psinc_S\left(\frac{k}{N}\right)\cdot psinc_T\left(\frac{l}{N}\right), & A \\ 0, & otherwise \end{cases} \tag{4}$$

where:

$$Condition\ A: 2k\ mod\ P = 0\ \&\ 2l\ mod\ P = 0\ \&\ (k+l)\ mod\ P = 0$$

$$f_1(k,l) = cos\left(\frac{2\pi L(k+l)}{2N}\right)$$

$$f_2(k,l) = cos\left(\frac{2\pi L(k-l)}{2N}\right)$$

$$psinc_W\left(\frac{x}{N}\right) = \frac{sin(\pi xW/N)}{sin(\pi x/N)}$$

(5)

Similarly, we perform the analysis on an encoded image based on the unbalanced shifting rule. In the unbalanced shifting rule, the shift position for a cluster corresponding to a given bit will use shifts in a single direction from the center position. For example, a one bit would shift up, and a zero bit would shift left. Thus, for the odd rows of halftone cells, the probabilistic model changes to

$$P\left(X_{i,j}=1 \cup Y_{i,j}=0\right)=\frac{1}{2}$$
$$P\left(X_{i,j}=0 \cup Y_{i,j}=1\right)=\frac{1}{2} \tag{6}$$

The probability distribution for the even rows of halftone cells is the same with that for the odd rows of halftone cells.

The expectation of magnitude of G [k, l] is

$$\mathscr{E}\left(|G[k,l]|\right)=\begin{cases}\frac{1}{4}P^2\cdot f_3(k,l)\cdot psinc_S\left(\frac{k}{N}\right)\cdot psinc_T\left(\frac{l}{N}\right), & B\\ 0, & otherwise\end{cases} \tag{7}$$

where:

$$Condition\ B: 2k\ mod\ P=0\ \&\ 2l\ mod\ P=0\ \&\ (k+l)\ mod\ P=0$$
$$f_3(k,l)=\sqrt{2+2\cdot cos\left(\frac{2\pi(k-l)L}{N}\right)} \tag{8}$$

Analysis of printed sample image

In this section, We captured printed data-bearing halftone pages. The data-bearing halftone image is generated based a constant-tone background, and printed in a laserJet printer. Then the printed image is captured by a phone camera.

If we directly apply DFT to the captured image and cover the DC component following the method in [4], strong concentration of power spectrum occur along the horizontal and vertical axes in the frequency domain, which increase the difficulty to locate the fundamental peaks, as shown in Figure 4. In order to solve this issue, we propose to apply a 2D Hanning window[10] on the captured image to reduce the effect of spatial domain truncation of the image. The resulting spectrum is shown in Figure 5. The effect is encouraging that the peaks in the frequency domain become much more obvious than before.

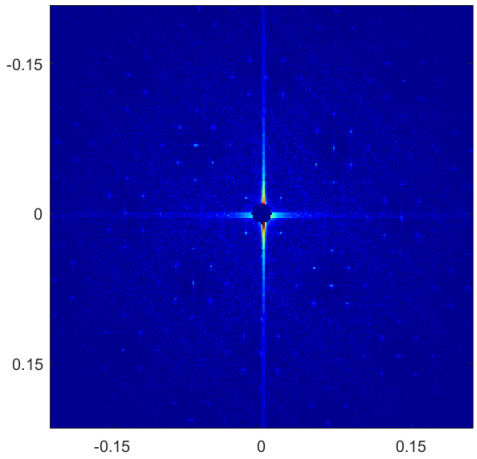

Figure 4. *Zoom-in of frequency domain of analysis region of captured image when no window is applied. The units of spatial frequency are cycles/pixel*

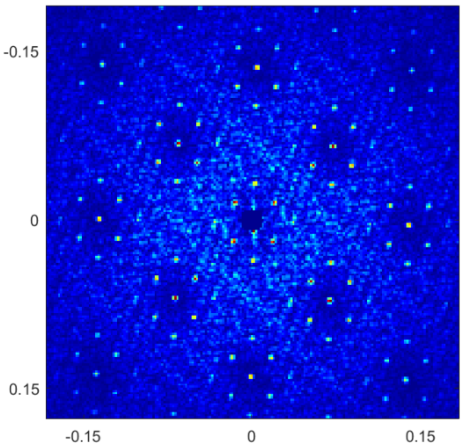

Figure 5. *Zoom-in of frequency domain of captured image after applying a Hanning window in the spatial domain*

After the captured image is rescaled based on the fundamental peaks in the frequency domain, the rescaled image halftone cell size should be equal to the printed image halftone cell size [4]. With this property, we are able to judge whether the fundamental peaks are located correctly by comparing the rescaled image halftone cell size and printed image cell size.

An Optimal Design of Data-Bearing Halftone Images

So far, we have made the assumption that the payload is random. However, this assumption is not suitable for all the cases in the application, especially for some extreme payloads. Thus, in this section, our goal is to develop a potential design of data-bearing halftone images which works for all kinds of payloads.

Corresponding to these changes, we need to update the probabilistic model and calculate the peak distributions according to the new model.

Suppose in the payload, α is the ratio of number of bits 0 to the payload length. Suppose in the payload, β is the ratio of

number of bits 1 to the payload length. Then we have that

$$\alpha+\beta=1 \tag{14}$$

We apply balanced shifting rule. For the odd rows of halftone cells, the probabilistic model becomes:

$$\begin{aligned} P\left(X_{i,j}=1 \cup Y_{i,j}=0\right)&=\frac{1}{2}\alpha \\ P\left(X_{i,j}=-1 \cup Y_{i,j}=0\right)&=\frac{1}{2}\alpha \\ P\left(X_{i,j}=0 \cup Y_{i,j}=1\right)&=\frac{1}{2}\beta \\ P\left(X_{i,j}=0 \cup Y_{i,j}=-1\right)&=\frac{1}{2}\beta \end{aligned} \tag{9}$$

The probability distribution for the even rows of halftone cells is the same as that for the odd rows of halftone cells.

The image expression in the spatial domain is the same as that shown in Equation 3. Combined with the updated probabilistic model, the expectation of the magnitude of G[k, l] is

$$\mathscr{E}|G[k,l]| = \begin{cases} \frac{1}{2}P^2 \cdot f_4(k,l) \cdot psinc_S\left(\frac{k}{N}\right) \cdot psinc_T\left(\frac{l}{N}\right), & C \\ 0, & otherwise \end{cases} \tag{10}$$

where:

$$Condition\ C: 2k\ mod\ P=0\ \&\ 2l\ mod\ P=0\ \&\ (k+l)\ mod\ P=0$$
$$f_4(k,l)=\alpha\cdot cos(\frac{2\pi kL}{N})+\beta\cdot cos(\frac{2\pi lL}{N}) \tag{11}$$

We can simplify condition C in Equation 11 to

$$\begin{aligned} 2k=a\cdot P,\quad 2l=b\cdot P,\quad k+l=c\cdot P \\ (a,b,c\ are\ integers) \end{aligned} \tag{12}$$

We substitute Equation 12 into Equation 10

$$\begin{aligned} \mathscr{E}\left(|G[k,l]|\right)=&\frac{1}{2}P^2[\alpha\cdot cos\left(\pi\frac{aL}{M}\right)+\beta\cdot cos\left(\pi\frac{2cL}{M}\right)cos\left(\pi\frac{aL}{M}\right) \\ &+\beta\cdot sin\left(\pi\frac{2cL}{M}\right)sin\left(\pi\frac{aL}{M}\right)]\cdot psinc_S\left(\frac{\pi a}{M}\right)\cdot psinc_T\left(\frac{\pi b}{M}\right) \end{aligned} \tag{13}$$

Then, we find that if we select L/M = 1/2 (dot shifting distance is half of the cell size), Equation 13 can be simplified to:

$$\begin{aligned} \mathscr{E}\left(|G[k,l]|\right)=&\frac{1}{2}P^2\cdot(\alpha+\beta\cdot cos(\pi c))\cdot cos\left(\frac{\pi a}{2}\right)\cdot \\ &psinc_S\left(\frac{2\pi a}{M}\right)\cdot psinc_T\left(\frac{2\pi b}{M}\right) \\ \leq&\frac{1}{2}P^2\cdot cos\left(\frac{\pi a}{2}\right)\cdot psinc_S\left(\frac{2\pi a}{M}\right)\cdot psinc_T\left(\frac{2\pi b}{M}\right) \end{aligned}$$

From Equation 12 and Equation 14, we can tell that when halftone cell size M is larger than a threshold value C, the maximum peak always locates at the position where $k=0$, $l=2P$ (which is $a=0, b=4$, from Equation 12) in the frequency domain no matter how the payload changes. The fundamental peak locates at the position where $k=1/2\cdot P$, $l=1/2\cdot P$ (which is $a=1, b=1$, from Equation 12). The reason why M is required to be larger than a threshold value C (for example, when the payload length is 67, $C=22$, $M\geq 22$) is that the values of last two terms in Equation 14 will change very little when a, c change from $a=1$, $b=1$ to $a=4$, $b=0$ with a large M value.

The threshold value C is calculated using Equation 15 where

l is payload length.

$$\frac{psinc_S\left(\frac{4}{C}\right)}{psinc_S\left(\frac{1}{C}\right)psinc_T\left(\frac{1}{C}\right)}=\frac{l-2}{l} \tag{15}$$

Equation 15 can be solved by iteration from an initial value. Assuming the halftone cell size M is equal to or greater than the threshold value C, a potential solution for locating the fundamental peaks in the 2D Fourier domain is to locate the peaks with maximum magnitude in the RMPS. Then according to the geometric relationship between RMPS and 2D Fourier domain, we can locate the fundamental peaks in the 2D Fourier domain based on the maximum peaks location in the RMPS.

Results

Validation of theoretical analysis via empirical analysis

We generate digital data-bearing halftone images using a random payload and apply Discrete Fourier Transform on the images.

Below is one of the examples where we adopt RMPS to compare the peak distribution predicted by theoretical analysis to that based on the DFT of the digital halftone image (the empirical result). The image is encoded with balanced shifted dot clusters. In this example, $N=480$, $S=2$, $T=2$, $M=24$, $L=6$. Note that these parameters don't satisfy the condition for which the maximum peak in the RMPS occurs at the fundamental frequency. The theoretical case in Figure 7 and the empirical result, which is in Figure 6, are consistent with what we expect. The primary difference between the RMPSs shown in Figure 6 and 7 is that the RMPS in Figure 6 has a significant baseline component, whereas the RMPS in Figure 7 has no baseline component. We hypothesize that this is due to the fact that Figure 6 is based on the DFT of a single sample function from the random process, whereas Figure 7 is based on an ensemble average over all realizations of the random process.

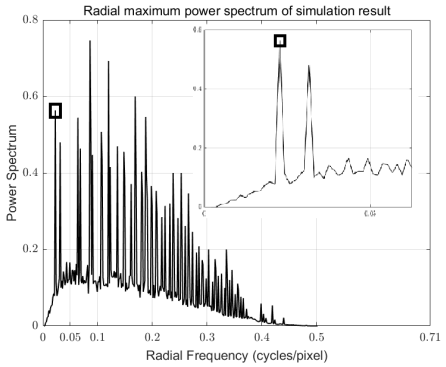

Figure 6. *Empirical RMPS based on the DFT of the digital halftone (The black box locates the fundamental peak. The upper right corner shows a close-up view of the fundamental peak)*

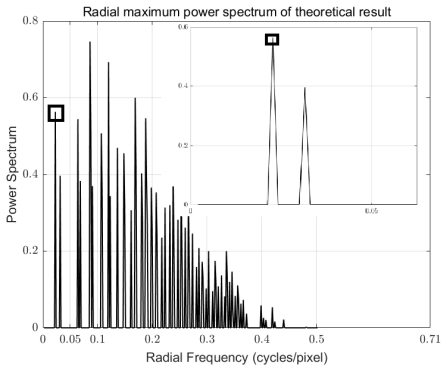

Figure 7. *Theoretical RMPS based on Equation 15 (The black box locates the fundamental peak. The upper right corner shows a close-up view of the fundamental peak)*

Validation of theoretical analysis via empirical analysis based on real captured images

Figure 8 shows the RMPS computed from a captured image of a printed version of the digital halftone on which the RMPS in Figure 7 is based. Due to the influence of the capture angle, light source, and capture distance, the peak distributions in the captured image is not exactly the same as that in the theoretical case shown in Figure 7. However, we are still able to achieve the conclusion that the first 5 peaks in the RMPS obey the same trends in both theoretical analysis and the real captured images. In fact, the peak with maximum value appears at the 5th peak in the RMPSs calculated from theoretical model(Equations 4 and 5)(Figure 7), via the DFT of the digital halftone (Figure 6) and the DFT of the printed and captured halftone pattern (Figure 8).

Validation of optimal design via simulation

For all possible payloads we tested, we find that when the carrier dot clusters' shifting distance is half of the printed cell size and the halftone cell size is greater than or equal to the threshold C given by the solution of Equation 15, the location of the peaks in the RMPS with largest magnitude is fixed no matter how the other parameters vary. The location of the peaks in the 2D Fourier domain corresponding to the fundamental frequency can be predicted based on the geometric relationship between the RMPS and

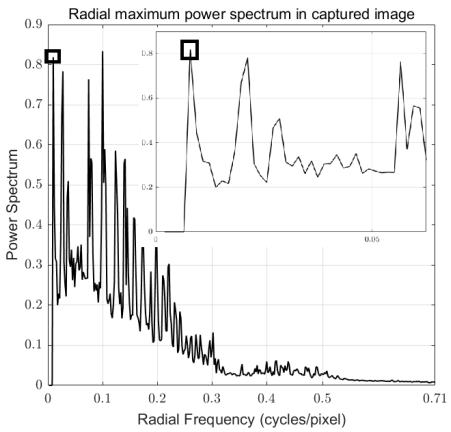

Figure 8. *RMPS of halftone pattern calculated from the DFT of the printed and captured image (The black box locates the fundamental peak. The upper right corner shows a close-up view of the fundamental peak)*

the 2D Fourier domain. This behavior holds for all payloads, even for extreme payloads. This result can be used as the basis for a potential optimal design of a data-bearing halftone image.

In this section, we use 3 different kinds of payloads covering different cases of payloads to illustrate our conclusion. The payload length is 67. The first payload consists of 66 bit one and 1 bit zero. The second payload consists of 57 bit one and 10 bit zero. The third payload consists of 33 bit one and 34 bit zero. These 3 payloads are respectively encoded into 3 fixed gray level images based on the balanced shifting rule. The 2D DFT is then applied to the encoded halftone image. We use the RMPS to observe the peaks location in the frequency domain. In this example, $N = 480$, $S = 2$, $T = 2$, $M = 24$, $L = 6$. These parameter values satisfy the optimal design rule that were started earlier.

From the result plots (Figures 9, 10, and 11), two predictions which we make are confirmed:

1. When the payload varies (the ratio of number of bit one to the number of bit zero in the payload varies), the fundamental peak magnitude changes dramatically, especially when the number of bit one and bit zero is similar ($|A - B|$ is small). It makes hard for us to locate the fundamental peaks directly.

2. When the payload varies (except when it consists of bit one or bit zero exclusively), if we select L/M = 1/2, the location in the RMPS of the peak with maximum magnitude never changes. Hence, as the location of the peak with maximum magnitude is fixed, we can predict the location of the fundamental peaks in the 2D DFT of the data-bearing halftone pattern based on the geometric relationship between the 2D DFT and the RMPS. Instead of setting a threshold to locate the four fundamental peaks in the 2D frequency domain, we can accurately locate one fundamental peak in the 2D DFT by using the relationship between the fundamental peak and the peak with maximum magnitude in the RMPS. Based on the symmetry property, we can locate the other three fundamental peaks in the 2D DFT accurately, as well.

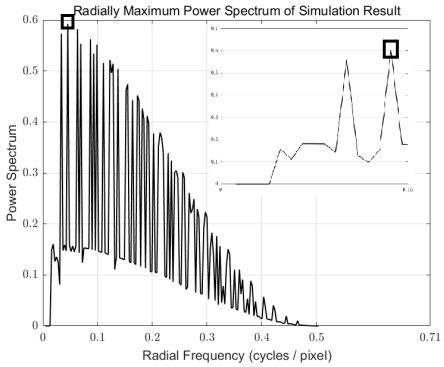

Figure 9. *RMPS for 1st payload (The black box locates the maximum peak. The upper right corner shows a close-up view of the maximum peak)*

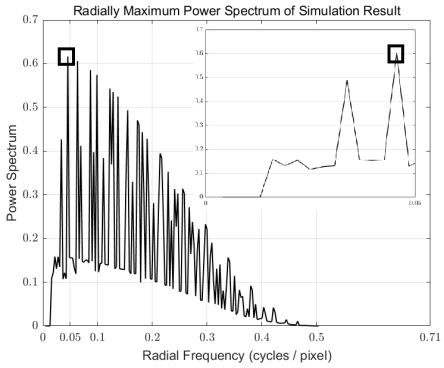

Figure 10. *RMPS for 2nd payload (The black box locates the maximum peak. The upper right corner shows a close-up view of the maximum peak)*

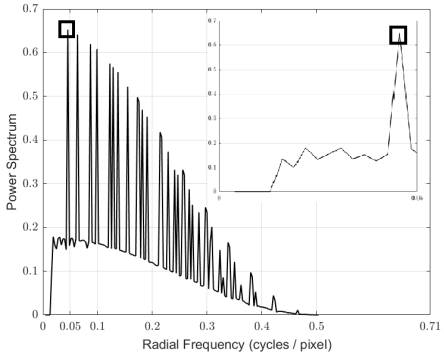

Figure 11. *RMPS for 3rd payload (The black box locates the maximum peak. The upper right corner shows a close-up view of the maximum peak.)*

Conclusion

Our work provides a theoretical analysis of the peak distributions in the frequency domain of data-bearing halftone images. Based on the developed theoretical system of data-bearing halftone images, we can predict how they will be influenced by different shifting rules and different design parameters. We perform experiments to validate the results. An optimal design is provided, based on a its theoretical proof. The optimal design can be applied in practice.

References

[1] R. Ulichney, M. Gaubatz, and S. Simske, Fast mobile stegatone detection using the frequency domain, NIP & Digital Fabrication Conference. Society for Imaging Science and Technology, vol. 2014, pg. 237. (2014).

[2] R. Ulichney, M. Gaubatz, and S. Simske, Encoding information in clustered-dot halftones, NIP & Digital Fabrication Conference. Society for Imaging Science and Technology, vol. 2010, pg. 602. (2010).

[3] O. Bulan, V. Monga, G. Sharma, and B. Oztan, Data embedding in hardcopy images via halftone-dot orientation modulation, Proc. SPIE: Security, Forensics, Steganography, and Watermarking of Multimedia Contents X, vol. 6819, pg. 68190C, (2008).

[4] R. Ulichney, M. Gaubatz, and S. Simske, Circular coding for data embedding, NIP & Digital Fabrication Conference. Society for Imaging Science and Technology, vol. 2013, pg. 142. (2013).

[5] Y.Y Chen, R. Ulichney, M. Gaubatz, S. Pollard, C. J. Tai and J. P. Allebach, Stegatone performance characterization, Media Watermarking, Security, and Forensics. International Society for Optics and Photonics, Vol. 8665, pg. 86650Q (2013)

[6] S. Pollard, R. Ulichney, M. Gaubatz, Recovering planar projection of printed cluster-dot halftones, IEEE International Conference on Image Processing. (2014).

[7] C. J. Tai, R. Ulichney, and J. P. Allebach, Effects on Fourier peaks used for periodic pattern detection. Electronic Imaging, Color Imaging XXIII: Displaying, Processing, Hardcopy, and Applications, vol. 13, pg. 1. (2016)

[8] R. Ulichney, Dithering with blue noise, Proc. IEEE, pg. 56. (1988).

[9] Y. Sun, R. Ulichney, M. Gaubatz, S. Pollard, S. Simske, and J. Allebach, Analysis of a Visually Significant Bar Code System Based on Circular Coding, Electronic Imaging, Color Imaging XXIII: Displaying, Processing, Hardcopy, and Applications, vol. 16, pg. 430. (2018).

[10] Oppenheim, Alan. V, Ronald W. Schafer, and John R. Buck, Discrete-Time Signal Processing, Upper Saddle River, NJ: Prentice Hall. (1999).

Author Biography

Ziyi Zhao received his BS in Naval Architecture and Ocean Engineering from Shanghai JiaoTong University from China (2015). He is currently a PhD student, working as an image processing research assistant with Prof. Jan Allebach, in the School of Electrical and Computer Engineering at Purdue University. His research interests are in image information embedding and digital image security, etc. He has been working on the project of circular coding sponsored by HP Labs.